Systematic Analysis of the Mechanisms of Virus-Triggered Type I IFN Signaling Pathways through Mathematical Modeling

Wei Zhang and Xiufen Zou

Abstract—Based on biological experimental data, we developed a mathematical model of the virus-triggered signaling pathways that lead to induction of type I IFNs and systematically analyzed the mechanisms of the cellular antiviral innate immune responses, including the negative feedback regulation of ISG56 and the positive feedback regulation of IFNs. We found that the time between 5 and 48 hours after viral infection is vital for the control and/or elimination of the virus from the host cells and demonstrated that the ISG56-induced inhibition of MITA activation is stronger than the ISG56-induced inhibition of TBK1 activation. The global parameter sensitivity analysis suggests that the positive feedback regulation of IFNs is very important in the innate antiviral system. Furthermore, the robustness of the innate immune signaling network was demonstrated using a new robustness index. These results can help us understand the mechanisms of the virus-induced innate immune response at a system level and provide instruction for further biological experiments.

Index Terms—Signaling pathways, mathematical modeling, negative feedback, positive feedback, robustness

1 Introduction

In recent years, the application of computational and systems biology tools to understand the molecular mechanisms of the signaling pathways of innate immunity has attracted the attention of many researchers because it is now recognized that the innate immune response plays a central role in the elimination of most pathogens without necessarily requiring the activation of adaptive immunity [1], [2], [3]. By combining quantitative data with mathematical models, the control mechanism of the IFN-induced JAK-STAT signaling pathways, the identification of a crucial factor in the IFN-α-induced pathway and the dynamic properties of the transcriptional factor NF-κB-related signaling pathways have been extensively studied [4], [5], [6], [7], [8], [9], [10], [11].

To reveal the detailed mechanism and the hidden dynamics of positive and negative feedback regulation in the innate immune signaling pathways, we developed an ordinary-differential-equations (ODEs) model of the virus-triggered type I IFN signaling pathways. Based on a previous model that focused on the early phase of the response, which results in the production of IFN-β [12], and a simplified delayed model that focused on a systematic dynamical analysis of this signaling pathway [13], in this study, we extended the simplified model by adding several important proteins to the pathways, a positive feedback regulation of the IFN proteins that leads to the transcription of IRF7 via the JAK-STAT pathway during the late phase of viral infection and a negative feedback regulation of ISG56 [14]. The hybrid genetic algorithm was used to identify the parameters of the ODEs. The negative feedback mechanism mediated by ISG56 and the positive feedback regulation of IFN were investigated. The robustness of the signaling network was also analyzed.

2 Signaling Pathways and Mathematical Model

2.1 Signaling Pathways

In response to viral infection, dsRNA interacts with the RNA-helicase domain of RIG-1 or MAD5 [15], [16], [17], [18], [19], [20]. The caspase-recruitment domain of RIG-1 or MAD5 transmits signals to the CARD modules of VISA, which interacts with MITA to form the complex VISA_MITA that mediates the phosphorylation of MITA [21], [22]. The phosphorylated MITA activates TBK1, and this activation leads to the phosphorylation of IRF3 and IRF7. In addition, phosphorylated MITA triggers the activation of NF-κB through the IKK proteins, and the activated NF-κB is translocated to the nucleus to trigger IFN mRNA induction [23]. At the same time, the phosphorylated IRF3 and IRF7 form homo- or heterodimers and are translocated to the nucleus to trigger IFN mRNA induction, which leads to the production of type I IFNs [14]. The type I IFNs induce the transcription of IFN-stimulated genes, such as ISG56; some antiviral proteins and IRF7 are also induced by IFN-mediated signaling pathways [24], [25], [26], [27]. The induced ISG56 inhibits the activation of MITA by targeting the formation of VISA_MITA and inhibits the activation of TBK1 by targeting the formation of MITA_TBK1 [28]. The IFN-induced antiviral proteins inhibit virus replication by target the virus RNA [29], [30]. The simplified diagram of the virus-induced type I IFN signaling pathways is depicted in Fig. 1.

• *The authors are with the School of Mathematics and Statistics, Wuhan University, Wuhan, Hubei Province, China 430072. E-mail: xfzou@whu.edu.cn.*

Manuscript received 16 Sept. 2012; revised 28 Mar. 2013; accepted 5 Apr. 2013; published online 10 Apr. 2013.
For information on obtaining reprints of this article, please send e-mail to: tcbb@computer.org, and reference IEEECS Log Number TCBB-2012-09-0249. Digital Object Identifier no. 10.1109/TCBB.2013.31.

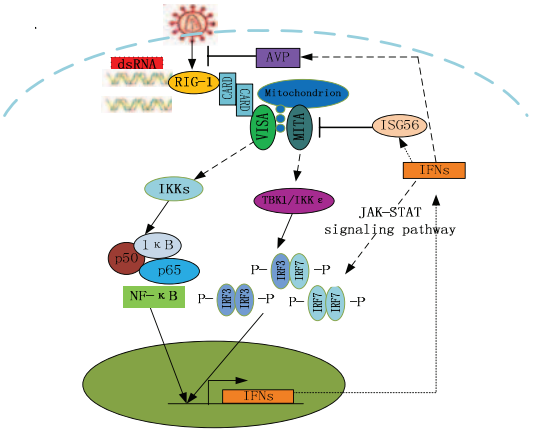

Fig. 1. Schematic diagram of virus-triggered type I IFN signaling pathways, dsRNA in the cytoplasm activates the RIG-1/MDA5 mediated the activation of NF-κB and IRF3/7, leading to the transcription of type I IFN gene (IFN-α/β), including all key components considered in the model ([14], [20], [21], [22], [24], [28]).

2.2 The Mathematical Model

Our model only considers those components that are involved in the interactions and dynamic processes that were found to be most important through experimental observations. The reaction scheme of the signaling pathways leading to the induction of IFN-β that were used to build the mathematical model is depicted in Fig. 2. To describe the mechanism of the ISG56 inhibition of MITA-VISA and MITA-TBK1, we introduced the parameter α, which varies in the range of [0, 1], to the model. The boundary values 0 and 1 of this parameter correspond to the ISG56 inhibition of only MITA-VISA and only MITA-TBK1, respectively.

Due to the complexity of the signaling networks, the following assumptions were made:

1. The activation and phosphorylation of a protein by another protein was described in a linear form.
2. The phosphorylated IRF3 and IRF7 translocate into the nucleus in the form of a homodimer or a heterodimer. These dimers then induce the transcription of IFN-β. Thus, we describe these proteins in a multiplication form. We also assume that the dimer and the process that activates NF-κB to induce the transcription of IFN-β in the nucleus follow Michaelis-Menten kinetics.
3. We consider the differences between the cytoplasmic and nuclear volumes in HEK293 cells; accordingly, a scaling factor k_v (ratio of the cytoplasmic volume and to the nuclear volume) was introduced. The nuclear import and export rates are proportional to the cytoplasmic and nuclear concentrations, respectively.

The mathematical model of the network is as follows:

$$
\begin{aligned}
d[Virus]/dt &= k_1[Virus]/(1+a_1[Avp]^{n_1}) - d_1[Virus]\\
d[MITA]/dt &= k_2[Virus]/(1+\alpha a_2[ISG56]^{n_2}) - d_2[MITA]\\
d[IKKs]/dt &= k_3[VISA] - d_3[IKKs]\\
d[NF\kappa B]/dt &= k_4[IKKs] - d_4[NF\kappa B]\\
d[TBK1]/dt &= k_5[VISA]/(1+(1-\alpha)a_5[ISG56]^{n_2})\\
&\quad - d_5[TBK1]
\end{aligned}
$$

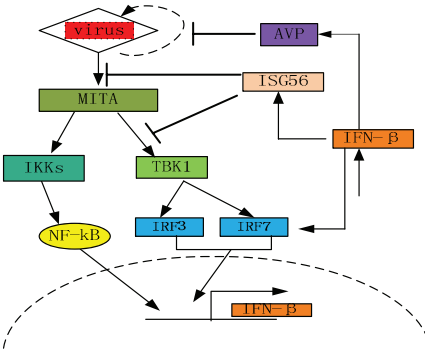

Fig. 2. A simplified reaction scheme considered in the mathematical model. Two possible mechanisms of ISG56 mediated the virus-triggered type I IFNs induction, the ISG56 inhibit the activation of MITA through disrupt the VISA-MITA interaction and inhibit the activation of TBK1 through disrupt the MITA-TBK1 interaction.

$$
\begin{aligned}
d[IRF3]/dt &= k_6[TBK1] - d_6[IRF3]\\
d[IRF7]/dt &= k_7[TBK1] + k_{71}[IFN\beta]/k_v/(1+a_7[IFN\beta]/k_v)\\
&\quad - d_7[IRF7]\\
d[IFN\beta]/dt &= k_v(k_8[NF\kappa B]^{n_3}/(1+a_{80}[NF\kappa B]^{n_3})\\
&\quad + k_{81}[IRF3]^{n_4}/(1+a_{81}[IRF3]^{n_4})\\
&\quad + k_{82}[IRF3][IRF7]/(1+a_{82}[IRF3][IRF7])\\
&\quad + k_{83}[IRF7]^{n_4}/(1+a_{83}[IRF7]^{n_4})) - d_8[IFN\beta]\\
d[ISG56]/dt &= k_9[IFN\beta]/k_v - \alpha k_{91}[MITA][ISG56]\\
&\quad - (1-\alpha)k_{92}[TBK1][ISG56] - d_9[ISG56]\\
d[Avp]/dt &= k_{10}[IFN\beta]/k_v - k_{11}[Virus][Avp] - d_{10}[Avp].
\end{aligned}
$$

The definitions of all of the parameters in the model are described in the first and second columns of Table 1.

3 Optimization Estimation and Sensitivity Analysis of the Parameters

3.1 A Hybrid Genetic Algorithm

To analyze the dynamical behavior of the signaling pathways based on the model, identification of the parameters in the nonlinear differential equations is critical. Some of the parameters can be collected by experiments, but the parameters for most processes are not directly accessible. Existing biochemical data usually originate from different experimental settings, cell types and states of cells and, therefore, not be automatically trusted and used for quantitative models. So accurate and reliable quantification of the parameters is essential for the development of predictive models and therefore parameter estimation is a hot topic in systems biology.

In this study, the parameter estimation was converted into an optimization problem, that is, to find the optimal parameter set that minimize the error between the simulation results and experimental data. Because the published data contain two classes of data, one is time series data of ISG56 activity; another is the inhibitory effect of ISG56 on IFN-β expression in the signaling pathways [28]. Mathematically, the object function contains two parts, the first part is the error between the simulation results and time series experimental data and the second part is the inhibitory effect error between experimental data and simulation results. The formulation can be expressed as

TABLE 1
The Optimal Parameters of the Model

Process	Paramter	Value	Units	Remarks
virus replication	k_1	8.769e-05	s^{-1}	Fitted
MITA induction	k_2	4.2975 e-04	s^{-1}	Fitted
IKKs induction	k_3	1.4776e-05	s^{-1}	Fitted
NF_κB induction	k_4	6.9658e-05	s^{-1}	Fitted
TBK1 induction	k_5	1.337 e-04	s^{-1}	Fitted
IRF3 induction	k_6	1.1297 e-04	s^{-1}	Fitted
IRF7 induction	k_7	1.154 e-04	s^{-1}	Fitted
IRF7 induction	k_{71}	2.944 e-04	s^{-1}	Fitted
IFN-β induction	k_8	1.1142e-05	s^{-1}	Fitted
IFN-β induction	k_{81}	2.37e-05	s^{-1} nM^{-1}	Fitted
IFN-β induction	k_{82}	6.4e-07	s^{-1} nM^{-1}	Fitted
IFN-β induction	k_{83}	8.965e-07	s^{-1} nM^{-1}	Fitted
ISG56 induction	k_9	3.8 e-04	s^{-1}	Fitted
ISG56 associate with MITA	k_{91}	2.723e-05	s^{-1} nM^{-1}	Fitted
ISG56 associate with TBK1	k_{92}	4.89e-06	s^{-1} nM^{-1}	Fitted
AVP induction	k_{10}	1.1594e-04	s^{-1}	Fitted
AVP associate with virus	k_{11}	9.76e-06	s^{-1} nM^{-1}	Fitted
virus degradation	d_1	8.64e-05	s^{-1}	Fitted
MITA degradation	d_2	7.7236e-05	s^{-1}	Fitted
IKKs degradation	d_3	8.8133e-06	s^{-1}	Fitted
NF_κB degradation	d_4	4.185e-05	s^{-1}	Fitted
TBK1 degradation	d_5	4.27e-05	s^{-1}	Fitted
IRF3 degradation	d_6	4.2377e-05	s^{-1}	Esti-mated [1]
IRF7 degradation	d_7	3.782 e-04	s^{-1}	Esti-mated [2]
IFNs degradation	d_8	1.12 e-04	s^{-1}	Esti-mated [3]
ISG56 degradation	d_9	2.4244 e-04	s^{-1}	Fitted
AVP degradation	d_{10}	5.1316e-05	s^{-1}	Fitted
Inhibition constant	a_1	1.275 e-02	nM^{-3}	Fitted
Inhibition constant	a_2	1.18 e-01	nM^{-2}	Fitted
associate constant	a_{80}	3.2858e-05	nM^{-1}	Fitted
associate constant	a_{81}	7.45 e-03	nM^{-2}	Fitted
associate constant	a_{82}	1.62 e-03	nM^{-2}	Fitted
associate constant	a_{83}	2.1533e-05	nM^{-2}	Fitted
associate constant	a_7	4.313e-05	nM^{-1}	Fitted
Inhibition constant	a_5	5.13 e-03	nM^{-2}	Fitted
Scale factor	α	6.55 e-01		Fitted
Hill coefficient	n_1	3		assumed
Hill coefficient	n_2	2		assumed
Hill coefficient	n_3	1		assumed
Hill coefficient	n_4	2		assumed
Ratio of cytoplasm and nuclear volumes	k_v	2		assumed

[1] *The half-life of IRF3 is about 5h, in the virus-triggered innate immune response the IRF3 was targeted by the E3 ligase Ro52 (TRIM21) for degradation, so the degradation rate is a bit higher than normal [38, 39].*
[2] *The half-life of IRF7 is about 30min [40].*
[3] *Experimental data showed the half-life of IFN- β is about 1-3h depending on real situation and the typical value of IFN-β mRNA half-life is 2h [41, 42, 43].*

$$\min J(P) = w_1 \sum_{k=1}^{K} \sum_{j=1}^{m} \left(\frac{y_k^D(\tau_j) - y_k(\tau_j, P)}{\max\left(y_k^D(\tau_j)\right)} \right)^2 + w_2 \sum_{i=1}^{n} \frac{|a_i - b_i(P)|}{a_i}, \quad (1)$$

where $y_k^D(\tau_j)$ represents the measured data of component y_k at time τ_j, which was extracted using the ImageJ software from the experimental immunoblot data [28], and $y_k(\tau_j, P)$ is the simulation result of component y_k in the mathematical model at time τ_j with parameter set P. The quantities a_i and $b_i(P)$ denote the inhibitory effect obtained from the experimental data [28] and the simulation results with parameter set P, respectively. The inhibitory effect is calculated using the expression levels of the involved components (IFN-β and NF-κB) at 12 hours under the inhibition of ISG56 divided by the expression levels of the involved components (IFN-β and NF-κB) when ISG56 is knocked down. The parameter k is the number of different components ($k = 1, 2, \ldots, K$), j is the number of time-series points ($j = 1, 2, \ldots, m$) and i is the number of different experimental groups ($i = 1, 2, \ldots, n$). The parameters w_1 and w_2 corresponding to the weight coefficients of the two separate parts of the object function. In this study, we set w_1 and w_2 to 1, which indicates that these two parts have the same priority.

Based on the experimental data, the initial concentration of Sendai virus used was approximately 100 nM. We assumed that the expressed concentrations are proportional to the plasmid doses. We also assumed that the initial concentrations of NF-κB, IRF3/7, TBK1 and IFN-β are the same as in a previous study [12]. The remaining four modeled species were set to zero. We set the initial values of the parameter set based on the available literature values ([6], [8], [12], [31]).

Due to the complexity of parameter estimation in nonlinear dynamic models of biological systems, traditional optimization methods, such as Levenberg-Marquardt and Gauss-Newton et al., may fail to identify the global solutions [32]. The genetic algorithm is one of the most competitive stochastic methods for nonlinear optimization and parameter estimation [33]. Therefore, we used a genetic algorithm based on multiparameter crossover to solve the optimization problem (1). The detailed descriptions of the algorithm are given as follows, and the optimal parameter set obtained through the use of this algorithm is detailed in Table 1.

A genetic algorithm:
Step 1. Guess the initial parameters and generate initial population $P(0) = \{X_1(\theta), \ldots, X_N(\theta)\}$ based on the initial data $X_0(\theta)$ through $X_0(\theta) + (2^*\text{rand-}X_0(\theta))/3$, N is the population size and set generation index $\theta = 0$;
Step 2. REPEAT
(a) Evaluate (Calculate) the fitness $\{f_1(\theta), \ldots, f_N(\theta)\}$ of all individuals in $P(\theta)$ according to (1) in main text, sort them in increasing order, and record the smallest fitness $v(\theta)$ of the population $P(\theta)$;
(b) Apply the following steps to derive new population $P(\theta + 1) = \{X_1(\theta + 1), \ldots, X_N(\theta + 1)\}$;
(1) Randomly select N1 individuals $\{X'_1(\theta), \ldots, X'_{N1}(\theta)\}$ from population $P(\theta)$ to generate N_2 individuals by using the following crossover:

$$X_{new} = \sum_{i=1}^{N1} \mu_i X_i \,, \sum_{i=1}^{N1} \mu_i = 1, \quad \mu_i \in [-0.5, 1.5] \quad (2)$$

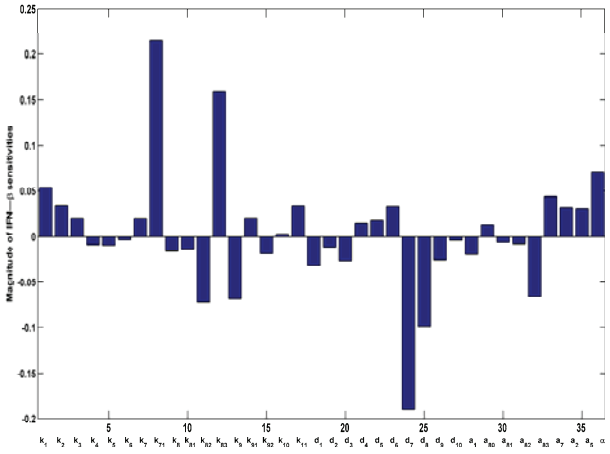

Fig. 3. Sensitivity analysis to the perturbation of parameters in the model.

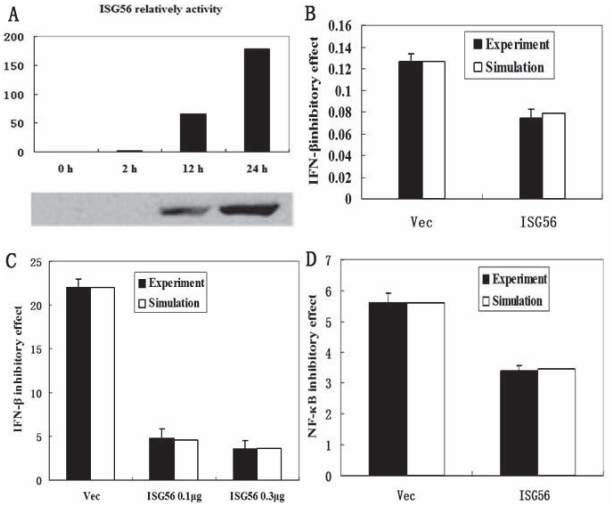

Fig. 4. Comparisons between the numerical simulation and the experimental results. (A) The upper figure is the simulation results of ISG56 activity and the below figure is the western blot array in the experiments [28]; (B) and (D) the inhibitory effects of ISG56 on the IFN-β mRNA and NF-κB, respectively, when the initial concentration of ISG56 is zero; and (C) the inhibitory effect of ISG56 on the IFN-β promoter when the initial concentrations of ISG56 are $0.1\ \mu g$ and $0.3\ \mu g$, respectively.

(quasi-linear combination is to expand the search space and can guarantee searching more extensive range, even including the boundary [34])
(2) Repeat Step 1 until a total of N_2 new individuals are obtained;
(3) Calculate the fitness of N_2 new individuals;
(4) Sort N_2 new individuals and N individuals in $P(\theta)$ in increasing order, and select N individuals with the smallest fitness to form the new population $P(\theta+1) = \{X_1(\theta+1), \ldots, X_N(\theta+1)\}$.
(c) Record the smallest fitness $v(\theta+1)$ of the population $P(\theta+1)$ and return to (a);
$(d)\theta := \theta + 1$;
UNTIL the stopping criteria $(\theta > K_1)$ fulfilled;
Step 3. Determine a set of the parameter values at which the cost function is minimal.
Step 4. Replace the initial seeds in Step 1 with the parameter values determined in Step 3.
Step 5. Iterate Steps 1-4 until the local cost values converge to a steady-state point and the parameter values at which the local cost value is minimal are considered to be the optimized parameters then output the optimized parameters.

3.2 Sensitivity Analysis

Sensitivity analysis is often conducted in the study of signaling pathways to understand how the system responds to changes in the parameters. Sensitivity analysis can also be exploited to identify molecules or mechanisms that have significant impact on the pathway dynamics under perturbed conditions.

To investigate the effects of parameter changes on the level of IFN-β activity, we performed a sensitivity analysis of the parameters using the partial rank correlation coefficient (PRCC) method [35], [36], [37]. The PRCC/LHS analysis is a global sensitivity analysis method that calculates the partial rank correlation coefficient for the model inputs (sampled by the Latin hypercube sampling method) and outputs. The calculated PRCC is a standardized sensitivity measurement between -1 and 1 such that a negative value indicates an inverse relationship between the parameter and output and a positive value indicates a positive relationship.

In this study, the sample size N was set to 1,000, and the order of magnitude of the perturbation was set to 0.1. The global sensitivities computed by the PRCC method are illustrated in Fig. 3. The sensitivity values profile the sensitivity of the input parameters to the expression of IFN-β. As shown in the figure, the parameter k_{71} (IFN-β-induced expression of IRF7) is the most sensitive parameter to the production of IFN-β. The next most sensitive parameters are the IRF7-induced expression of IFN-β (k_{83}) and the degradation rates of IRF7 (d_7) and IFN-β (d_8).

The results show that the most sensitive parameters are involved in the positive feedback loop, which indicates that the positive feedback mechanism is very important to the expression of IFN-β.

4 Numerical Experimental Results

4.1 Comparison of the Simulation Results with Experiment Observations

The negative control mechanism of ISG56 in the early system response is a mediator of negative feedback regulation of the cellular antiviral responses that help prevent a harmful excessive immune response. The experimental results from a previous study [23] suggest that the overexpression of ISG56 strongly inhibits the SeV-induced activation of the IFN-β promoter in a dose-dependent manner and that the knockdown of ISG56 promotes the virus-induced activation of NF-κB and the IFN-β promoter.

We used our mathematical model to simulate the inhibitory effects of ISG56 on the SeV-induced IFN-β signaling pathways. Fig. 4 demonstrates that the simulation results are consistent with the two types of experimental data, which were described in Section 3.1. The consistency between the experiment data and simulation result

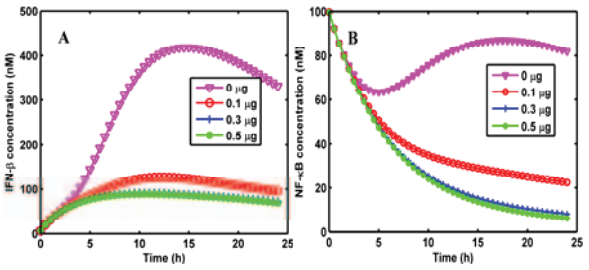

Fig. 5. The relationship between the initial dose of ISG56 plasmid and the inhibitory effects on IFN-β and NF-κB induction.

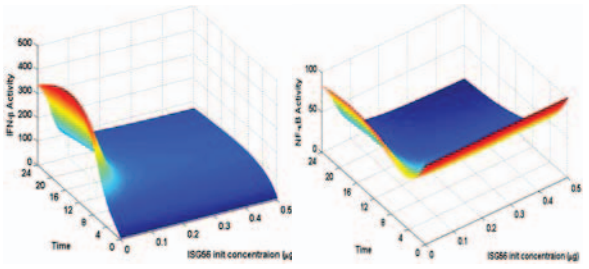

Fig. 6. The mesh diagrams of virus-triggered IFN-β and NF-κB induction with the increase of ISG56 initial concentration.

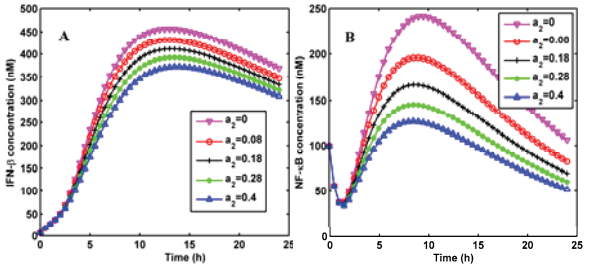

Fig. 7. Dynamic behavior of the IFN-β and NF-κB with the increasing of the negative feedback strength.

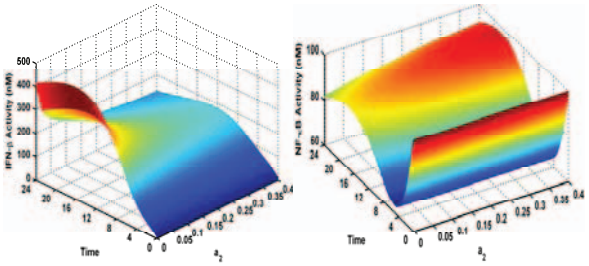

Fig. 8. The mesh diagrams of virus-triggered IFN-β and NF-κB induction with the increase of negative feedback strength.

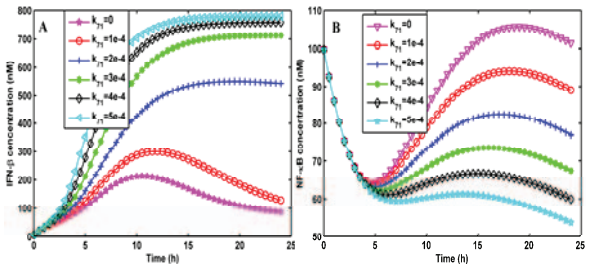

Fig. 9. Dynamic behavior of the IFN-β and NF-κB with the increasing of the positive feedback strength.

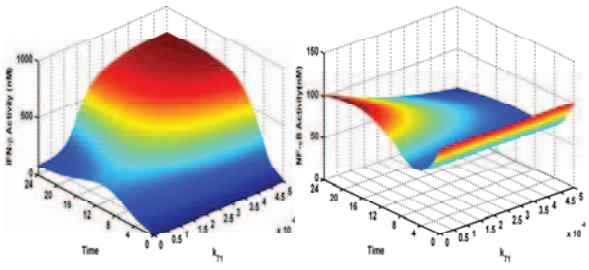

Fig. 10. The mesh diagrams of virus-triggered IFN-β and NF-κB induction with the increase of positive feedback strength.

indicated that the reasonability of the parameter estimation method and the reliability of the model.

4.2 Quantitative Relationship between the Inhibitory Effects of ISG56 and IFN-β Induction

To investigate the dose of ISG56 plasmid that gives the maximal inhibition of IFN-β induction, we simulated ISG56 plasmid doses ranging from 0 to 0.5 μg with a 0.1-μg dose interval. As shown in Fig. 5, the inhibitory effects are rapidly decreased with 0.1 μg of ISG56 plasmid, and the IFN-β and NF-κB activations reach a steady state when the initial concentration of ISG56 is approximately 0.3 μg. However, no difference was observed when the initial concentration of ISG56 was greater than 0.3 μg. To observe the inhibitory effects more clearly, we drew the corresponding mesh figure, which is shown in Fig. 6.

We further investigated how the strength of the negative feedback of ISG56, i.e., the parameter a_2, affects the expression of IFN-β. The numerical simulation results are depicted in Fig. 7. An increase in the value of a_2 decreased both IFN-β and NF-κB. However, the influence of the parameter a_2 on NF-κB is greater than that on IFN-β. The corresponding mesh diagrams are depicted in Fig. 8. In fact, the negative feedback inhibits the NF-κB and the IRF3/7 signaling pathways, which together mediate the induction of IFN-β. The results suggest that the positive feedback in the pathway may counteract the inhibitory effects on the induction of IFN-β.

4.3 Investigation of the Positive Feedback Regulation of the Network

The virus-triggered type I IFN signaling pathways feature both positive and negative feedback loops, both of which have essential roles in the regulation of the innate immune system.

The parameter k_{71} is the rate of IFN-β-induced IRF7 expression; thus, this parameter can be considered the strength of the positive feedback. As shown in Fig. 9A, the numerical simulations demonstrate that an increase in the strength of the positive feedback induces a rapid increase in IFN-β during the late phase of infection. In the early phase (before 5 hours), the level of the transcription factor NF-κB decreases. Moreover, the presence and strength of the positive feedback did not affect the induction of IFN-β. However, in the late phase of infection, the level of NF-κB is dramatically increased in the presence of positive feedback, but the amplitude of this increase decreased with increasing k_{71} (see Fig. 9B). The corresponding mesh diagrams are depicted in Fig. 10. These results demonstrate the importance of the regulation of NF-κB after 5 hours.

To investigate the dynamics of the positive feedback loop, we removed the positive feedback and conducted numerical

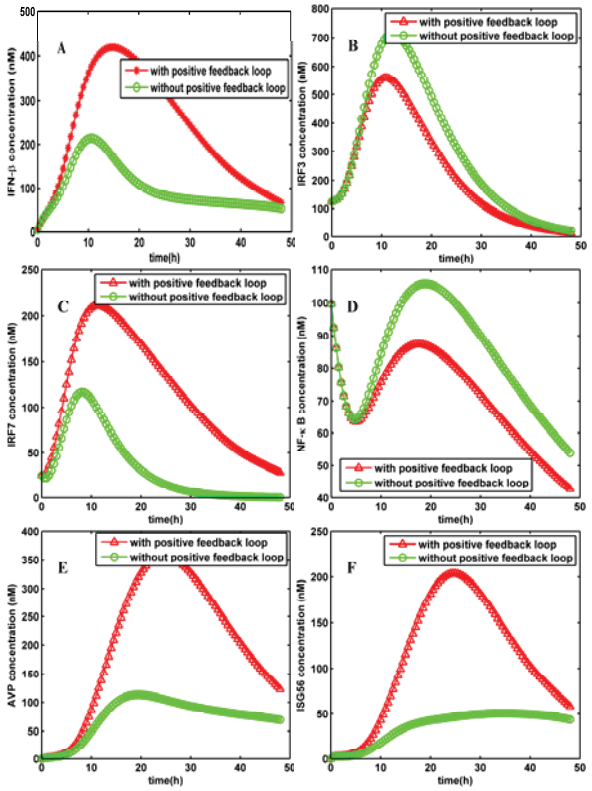

Fig. 11. The simulation of the positive feedback mechanism. "Without positive feedback loop" indicates that the positive feedback loop has been cutoff when IFN-β leads to the transcription of IRF7. The dynamic behavior of IFN-β, IRF3, IRF7, NF-κB, AVP, ISG56 with or without positive feedback are illustrated in the above A, B, C, D, E, and F, respectively.

simulations. Fig. 11 compares the results obtained in the presence and absence of the positive feedback loop. As shown in the figure, the IFN-β and IRF7 levels have the same influences by the positive feedback loop (see Figs. 11A and 11C), but the changes in the IRF3 and NF-κB levels are different from the changes in the IFN-β level (see Figs. 11B and 11D), which indicates that the expression of IFN-β is mainly regulated by phosphorylated IRF7. The results are consistent with previously published results ([15]).

High levels of IFN-α/β induce additional ISGF3 and the production of additional ISG56, which will lead to a stronger inhibition of the IRF3- and NF-κB-related signaling pathways. Moreover, during the late phase of viral infection, the expression levels of IRF3 and NF-κB in the presence of positive feedback are lower than those obtained in the absence of positive feedback. The concentrations of both IFN-β and IRF3 increase after the positive feedback comes into effect (after 5 hours of viral infection). In addition, the concentrations of IFN-β and IRF3 decrease after this initial rise and, approximately 48 hours after the beginning of the infection, reach almost the same level as that obtained in the absence of positive feedback. This switch, which is induced by the positive feedback, indicates that the time between 5 and 48 hours after the initiation of viral infection is vital for the control and/or elimination of the virus from the host cells.

Real biochemical networks have developed mechanisms to maintain their specificity when transmitting signals; these

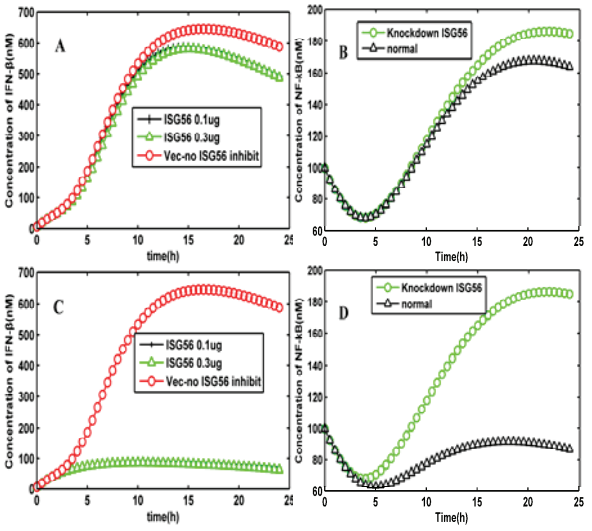

Fig. 12. The SeV-induced activation of the IFN-β and NF-κB with or without negative feedback of ISG56 under different initial concentration of ISG56 are as following: (A) and (B) randomly decreasing a_2 by $a_2 = a_2/2 + a_2{}^*\mathrm{rand}$ satisfied that $\alpha a_2 > (1-\alpha)a_5$; (C) and (D) randomly increasing a_5 by $a_5 = a_5 + a_5{}^*\mathrm{rand}$ satisfied $\alpha a_2 > (1-\alpha)a_5$; (A) and (C) the dynamic behavior of IFN-β as the increase of initial concentration of ISG56 or without the inhibition of ISG56; and (B) and (D) the dynamic behavior of NF-κB with or without negative feedback of ISG56.

mechanisms usually involve maintaining the ratio between the parameters in a certain mechanism within a range [44].

To analyze the effects of parameters on the signaling pathway, we performed a counterfactual analysis between parameters a_2 and a_5.

Assuming that $a_2 > a_5$ and $\alpha a_2 > (1-\alpha)a_5$, which indicates that MITA-associated ISG56 (STING) predominantly disrupts the interaction between MITA and VISA and inhibits the activation of the NF-κB and the IRF3 signaling pathways, it was found that ISG56 plays a small part in the disruption of the interaction between MITA and TBK1, which further inhibits the activation of IRF3 and mediates the expression of type I interferons (IFN-α and IFN-β).

If $a_2 < a_5$ and $\alpha a_2 < (1-\alpha)a_5$, there are two possible cases: decreasing parameter a_2 or increasing parameter a_5. For case one, the simulation results show that there is little effect on the IFN-β and NF-κB induction when the inhibition of ISG56 is knocked down and that there is no difference in the level of IFN-β when the initial concentration of ISG56 is increased (see Figs. 12A and 12B). For case two, the simulation results show that ISG56 effectively inhibits the induction of IFN-β and NF-κB, although the concentration of IFN-β becomes more stable as the initial concentration of ISG56 increases (see Figs. 12C and 12D). The simulation results indicate that the ISG56-induced inhibition of MITA activation is stronger than the ISG56-induced inhibition of TBK1 activation.

5 Robustness Analysis

Robustness is the maintenance of specific functionalities of the system in the presence of perturbations [45]. Real biochemical networks must be sufficiently robust to tolerate parameter and environmental variations such that the system can efficiently respond to small but persistent parameter and environmental perturbations. For a robust innate immune system, both signaling specificity and

complexity are required because excessive or prolonged cytokine production leads to inflammation and tissue damage. The IFN response is strictly regulated to avoid pathologic consequences, including autoimmunity [46].

We assume that the robustness of the innate immune system can be measured by determining the behavior or feature of a system as a function of a perturbation.

The innate immune system will exhibit excessive autoimmunity if the amount of IFN-β is above a certain threshold for over a certain threshold time. However, for a robust innate immune system, the virus-triggered induction of IFN-β should not remain below a specific threshold to ensure that the innate immune system is able to execute the functions that control the viral infection [47], [48].

To measure the immune response triggered by viral infection, we defined the state of the immune response C with the following formula:

$$C = \begin{cases} t|_{\max(y_r(t)) \geq \sigma \max(y_0(t))} > \beta t_0, & \text{excessive immunity,} \\ \sigma \max(y_0(t)) > \max(y_r(t)) > \lambda \max(y_0(t)), & \text{normal,} \\ \max(y_r(t)) \leq \lambda \max(y_0(t)), & \text{immunodenficiency,} \end{cases} \tag{3}$$

where $t_0 = t|y_0(t) > (\max(y_0(t)) - \Delta)$, $y_0(t)$ is the concentration of IFN-β under the optimal parameter set in Table 1 and $y_r(t)$ is the concentration of IFN-β when the parameters were perturbed. The maximum concentration of IFN-β is approximately 420 nM. Here, Δ is set to 10 nM, and time t_0 is approximately 4.5 hours, i.e., the concentration of IFN-β is greater than 410 nM for approximately 4.5 hours. The three parameters σ, β, and λ are the threshold values that were used to characterize the robustness of the system. We assume that an excessive immunity response occurs when the amount of IFN-β is above 10 percent of the normal maximum amount of IFN-β for over 50 percent of the normal maximum duration time. The system behavior indicates immunodeficiency when the maximum amount of IFN-β is less than 50 percent of the normal maximum amount. Therefore, the parameters in equation (3) were set to the following: $\sigma = 1.1$, $\beta = 1.5$, and $\lambda = 0.5$. We varied the value of each parameter from -30 to 30 percent of the normal value in 1 percent steps. The black box that is shown in Fig. 13 indicates which perturbed parameter sets yield excessive immunity or immunodeficiency.

A white box indicates that the induction of IFN-β was normal. The results show that almost half of the parameters could be increased and decreased by 30 percent of their normal magnitude without triggering overimmunity or immunodeficiency. However, several parameters were subject to strong one-sided limitations, i.e., when the perturbed parameters are higher or lower than a threshold value, the system behavior indicates an excessive immunity or an immunodeficiency response. The system behavior is robust to the perturbation of all of the parameters within the interval -7 to 9 percent of their normal values.

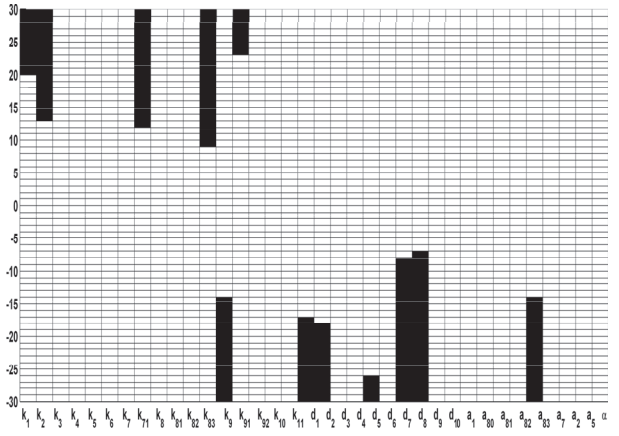

Fig. 13. Robustness of the model against parameter changes. The horizontal axis shows the parameters in the model and vertical axis shows the perturbation amplitude from -30 to 30 percent corresponding to each of the parameters. A black box means the system behavior is excessive immunity or immunodeficiency when the corresponding parameter is perturbed at certain amplitude while a white box means the system behavior is normal when the corresponding parameter is perturbed.

6 Conclusion

In the last few years, many positive and negative regulators that control the virus-triggered innate immune signaling pathways through different mechanisms or at multiple levels have been experimentally identified.

The innate immune signaling networks have proven difficult to characterize, and most of the data that has been accumulated on such mechanisms are qualitative in nature and scattered across different experimental contexts. It may not be possible to solve this problem through laboratory experiments due to the variations in environmental conditions, cell types, and applied methodologies.

Based on previous work, we developed a model of virus-triggered type I IFN production. In this model, we introduced a positive feedback regulation of the JAK-STAT pathway in the late phase of viral infection and an ISG56-mediated negative feedback regulation. We developed a simplified model and performed a detailed analysis of the negative and the positive feedback loops. The simulation results demonstrate that the model is reasonable. We showed that the ISG56-induced inhibition of MITA activation is stronger than the ISG56-induced inhibition of TBK1 activation. Through our numerical simulations, we further showed that the positive feedback of IRF7 induced by IFN-β in the late phase of infection contributes to the late-phase IFN-β induction, which is consistent with the results reported in the literature [36]. The analysis of the positive feedback using the model showed that the time between 5 and 48 hours after viral infection is vital for the control and/or elimination of the virus from the host cells. This finding may provide insights for the development of effective treatments against virus-induced diseases. Furthermore, we analyzed the robustness of the system by defining a new measure. This analysis demonstrated that the system behavior is robust to the perturbation of parameters within the interval -7 to 9 percent of their respective normal values.

The virus-triggered immune response is very complicated, and a large number of feedback mechanisms coordinately regulate the virus-triggered type I IFN production and cellular antiviral response. Due to the

limitations of available experimental data, our research only considered a basic model that captures the main features of the signaling pathway. Therefore, the model may exhibit limitations in the interpretation of the mechanistic details.

To analyze the robustness of the system in response to the perturbation of parameters, we proposed a new measure to differentiate between the normal state, overimmunity and immunodeficiency. This differentiation was accomplished by setting a threshold value that captured the main response properties of the system and may provide insights for further analysis. However, the definition is rough. Thus, the development of a more accurate definition of the robustness of the system needs additional in-depth research.

Further data-driven refinements of the mathematical model will need to be directed toward a more detailed understanding of the mechanisms that control the antiviral responses and avoid autoimmunity.

ACKNOWLEDGMENTS

This work was supported by the Chinese National Natural Science Foundation (No. 61173060), the Major Research Plan of the National Natural Science Foundation of China (No. 91230118), and the Independent Scientific Research Project of the Wuhan University Graduate Student (No. 2012201020205).

REFERENCES

[1] S.D. Shapira and N. Hacohen, "Systems Biology Approaches to Dissect Mammalian Innate Immunity," *Current Opinion in Immunology,* vol. 23, no. 1, pp. 71-77, 2011.

[2] D.E. Zak and A. Aderem, "Systems Biology of Innate Immunity," *Immunology Rev.,* vol. 227, no. 1, pp 264-282, 2009.

[3] A. Iwasaki and R. Medzhitov, "Regulation of Adaptive Immunity by the Innate Immune System," *Science,* vol. 327, no. 5963, pp. 291-295, 2010.

[4] Z.K. Zi, K.H. Cho, M.H. Sung, X. Xia, J. Zheng, and Z. Sun, "In Silico Identification of the Key Components and Steps in IFN-Gamma Induced JAK-STAT Signaling Pathway," *FEBS Letters,* vol. 579, no. 5, pp. 1101-1108, 2005.

[5] R.P. Soebiyanto, S.N. Sreenath, C.K. Qu, K.A. Loparo, and K.D. Bunting, "Complex Systems Biology Approach to Understanding Coordination of JAK-STAT Signaling," *Biosystems,* vol. 90, no. 3, pp. 830-842, 2007.

[6] E. Shudo, J. Yang, A. Yoshimuraand, and Y. Iwasa, "Robustness of the Signal Transduction System of the Mammalian JAK/STAT Pathway and Dimerization Steps," *J. Theoretical Biology,* vol. 246, no. 1, pp. 1-9, 2007.

[7] I. Swameye, T.G. Muller, J. Timmer, O. Sandra, and U. Klingmuller, "Identification of Nucleocytoplasmic Cycling as a Remote Sensor in Cellular Signaling by Databased Modeling," *Proc. Nat'l Academy of Sciences USA,* vol. 100, no. 3, pp. 1028-1033, 2003.

[8] T. Maiwald, A. Schneider, H. Busch, S. Sahle, N. Gretz, T.S. Weiss, U. Kummer, and U. Klingmuller, "Combining Theoretical Analysis and Experimental Data Generation Reveals IRF9 as a Crucial Factor for Accelerating Interferon Alpha-Induced Early Antiviral Signaling," *FEBS J.,* vol. 277, no. 22, pp. 4741-4754, 2010.

[9] J. Bachmann, A. Raue, M. Schilling, M.E. Böhm, C. Kreutz, and U. Klingmuller, "Division of Labor by Dual Feedback Regualtors Controls JAK2/STAT5 Signaling over Broad Ligand Range," *Molecular System Biology,* vol. 7, article 516, 2011.

[10] R. Cheong, A. Hoffmann, and A. Levchenko, "Understanding NF-κB Signaling via Mathematical Modeling," *Molecular System Biology,* vol. 4, article 192, 2008, doi: 10.1038/msb.2008.30.

[11] P.W. Sheppard, X.Y. Sun, J.F. Emery, R.G. Giffard, and M. Khammash, "Quantitative Characterization and Analysis of the Dynamic NF-κB Response in Microglia," *BMC Bioinformatics,* vol. 12, article 276, 2011.

[12] X.F. Zou, X.S. Xiang, Y. Chen, T. Peng, X.L. Luo, and Z.S. Pan, "Understanding Inhibition of Viral Proteins on Type I IFN Signaling Pathways with Modeling and Optimization," *J. Theoretical Biology,* vol. 265, pp. 691-703, 2010.

[13] J.Y. Tan, R.G. Pan, L. Qiao, X.F. Zou, and Z.S. Pan, "Modeling and Dynamical Analysis of Virus-Triggered Innate Immune Signaling Pathways," *PLoS ONE,* vol. 7, no. 10, article e48114, 2012.

[14] K. Honda and T. Taniguchi, "IRFs: Master Regulators of Signaling by Toll-Like Receptors and Cytosolic Pattern-Recognition Receptors," *Nat'l Rev. Immunology,* vol. 6, no. 9, pp. 644-658, 2006.

[15] E. Meylan, J. Curran, K. Hofmann, D. Moradpour, M. Binder, R. Bartenschlager, and J. Tschopp, "Cardif Is an Adaptor Protein in the RIG-I Antiviral Pathway and Is Targeted by Hepatitis C Virus," *Nature,* vol. 437, no. 7062, pp. 1167-1172, 2005.

[16] J. Andrejeva, K.S. Childs, D.F. Young, T.S. Carlos, N. Stock, S. Goodbourn, and R.E. Randall, "The V Proteins of Paramyxoviruses Bind the IFN-Inducible RNA Helicase, mda-5, and Inhibit Its Activation of the IFN-Beta Promoter," *Proc. Nat'l Academy of Sciences USA,* vol. 101, no. 49, pp. 17264-17269, 2004.

[17] V. Hornung, J. Ellegast, S. Kim, K. Brzozka, A. Jung, H. Kato, H. Poeck, S. Akira, K.K. Conzelmann, and M. Schlee, "50-Triphosphate RNA is the Ligand for RIG-I," *Science,* vol. 10, no. 314, pp. 994-997, 2006.

[18] L.G. Xu, Y.Y. Wang, K.J. Han, L.Y. Li, Z. Zhai, and H.B. Shu, "VISA Is an Adapter Protein Required for Virus-Triggered IFN-Beta Signaling," *Molecular Cell,* vol. 19, no. 6, pp. 727-740, 2005.

[19] T. Kawai, K. Takahashi, S. Sato, C. Coban, H. Kumar, H. Kato, K.J. Ishii, O. Takeuchi, and S. Akira, "IPS-1, an Adaptor Triggering RIG-I- and Mda5-Mediated Type I Interferon Induction," *Nat'l Immunology,* vol. 6, no. 10, pp. 981-988, 2005.

[20] R.B. Seth, L. Sun, C.K. Ea, and Z.J. Chen, "Identification and Characterization of MAVS, a Mitochondrial Antiviral Signaling Protein That Activates NF-kappaB and IRF3," *Cell,* vol. 122, no. 5, pp. 669-682, 2005.

[21] H. Ishikawa and G.N. Barber, "STING Is an Endoplasmic Reticulum Adaptor That Facilitates Innate Immune Signaling," *Nature,* vol. 455, no. 7213, pp. 674-678, 2008.

[22] B. Zhong, Y. Yang, S. Li, Y.Y. Wang, Y. Li, F. Diao, C. Lei, X. He, L. Zhang, P. Tien, and H.B. Shu, "The Adaptor Protein MITA Links Virus-Sensing Receptors to IRF3 Transcription Factor Activation," *Immunity,* vol. 29, no. 4, pp. 538-550, 2008.

[23] I.E. Wertz, K.M. O'Rourke, H. Zhou, M. Eby, L. Aravind, S. Seshagiri, P. Wu, C. Wiesmann, R. Baker, D.L. Boone, A. Ma, E.V. Koonin, and V.M. Dixit, "De-ubiquitination and Ubiquitin Ligase Domains of A20 Downregulate NF-Kappab Signaling," *Nature,* vol. 430, no. 7000, pp. 694-699, 2004.

[24] M. Sato, N. Hata, M. Asagiri, T. Nakaya, T. Taniguchi, and N. Tanaka, "Positive Feedback Regulation of Type I IFN Genes by the IFN-Inducible Transcription Factor IRF-7," *FEBS Letters,* vol. 441, no. 1, pp. 106-110, 1998.

[25] T. Taniguchi and A. Takaoka, "A Weak Signal for Strong Response: Interferon-α/β Revisited," *Nat'l Rev. Molecular Cell Biology,* vol. 2, no. 5, pp. 378-386, 2001.

[26] I. Marie, J.E. Durbin, and D.E. Levy, "Differential Viral Induction of Distinct Interferon-α Genes by Positive Feedback through Interferon Regulatory Factor-7," *EMBO J.,* vol. 17, no. 22, pp. 6660-6669, 1998.

[27] T. Taniquchi and A. Takaoka, "The Interferon α/β System in Antiviral Responses: A Multimodal Machinery of Gene Regulatory by the IRF Family of Transcription Factors," *Current Opinion in Immunology,* vol. 14, no. 1, pp. 111-116, 2002.

[28] Y. Li, C. Li, P. Xue, B. Zhong, A.P. Mao, Y. Ran, H. Chen, Y.Y. Wang, F.Q. Yang, and H.B. Shu, "ISG56 Is a Negative-Feedback Regulator of Virus-Triggered Signaling and Cellular Antiviral Response," *Proc. Nat'l Academy of Sciences USA,* vol. 106, no. 19, pp. 7945-7950, 2009.

[29] M.J. De Veer, M. Holko, M. Frevel, E. Walker, S. Der, J.M. Paranjape, R.H. Silverman, and B.R. Williams, "Functional Classification of Interferon-Stimulated Genes Identified Using Microarrays," *J. Leukocyte Biology,* vol. 69, no. 6, pp. 912-920, 2001.

[30] R.B. Seth, L.J. Sun, and Z.J.J Chen, "Antiviral Innate Immunity Pathways," *Cell Research,* vol. 16, pp. 141-147, 2006.

[31] J. Smieja, M. Jamaluddin, A.R. Brasier, and M. Kimmel, "Model-Based Analysis of Interferon-Beta Induced Signaling Pathway," *Bioinformatics,* vol. 24, no. 20, pp. 2363-2369, 2008.

[32] M. Rodriguez-Fernandez, J.A. Egea, and J.R. Banga, "Novel Metaheuristic for Parameter Estimation in Nonlinear Dynamic Biological Systems," *BMC Bioinformatics,* vol. 7, article 483, 2006.
[33] E. Balsa-Canto, J.R. Banga, J.A. Egea, A. Fernandez-Villaverde, and G.M de Hijas-Liste, "Global Optimization in Systems Biology: Stochastic Methods and Their Applications," *Advances in Experimental Medicine and Biology,* vol. 736, pp. 409-424, 2012.
[34] X. Zou and L. Kang, "Fast Annealing Genetic Algorithm for Multi-Objective Optimization Problems," *Int'l J. Computer Math.,* vol. 82, no. 8, pp. 931-940, 2005.
[35] N. Draper and H. Smith, *Applied Regression Analysis,* second ed. Wiley, 1981.
[36] Y. Zheng and A. Rundell, "Comparative Study of Parameter Sensitivity Analyses of the TCR-Activated Erk-mapk Signalling Pathway," *IEEE Proc. Systems Biology,* vol. 153, no. 4, pp. 201-211, 2006.
[37] S. Marino, I.B. Hogue, C.J. Ray, and D.E. Kirschner, "A Methodology for Performing Global Uncertainty and Sensitivity Analysis in Systems Biology," *J. Theoretical Biology,* vol. 254, no. 1, pp. 178-196, 2008.
[38] J. Hiscott, "Triggering the Innate Antiviral Response through IRF-3 Activation," *J. Biological Chemistry,* vol. 282, no. 21, pp. 15325-15329, 2007.
[39] R. Higgs, J. Ní Gabhann, N. Ben Larbi, E.P. Breen, K.A. Fitzgerald, and C.A. Jefferies, "The E3 Ubiquitin Ligase Ro52 Negatively Regulates IFN-β Production Post-Pathogen Recognition by Polyubiquitin-Mediated Degradation of IRF3," *J. Immunology,* vol. 181, no. 3, pp. 1780-1786, 2008.
[40] A. Prakash and D.E. Levy, "Regulation of IRF7 through Cell Type-Specific Protein Stability," *Biochemical and Biophysical Research Comm.,* vol. 342, no. 1, pp. 50-56, 2006.
[41] E. Yang, E. van Nimwegen, M. Zavolan, N. Rajewsky, M. Schroeder, M. Magnasco, and J.E. Darnell, "Decay Rates of Human mRNAs: Correlation with Functional Characteristics and Sequence Attributes," *Genome Research,* vol. 13, no. 8, pp. 1863-1872, 2003.
[42] J. Hu, S.C. Sealfon, F. Hayot, C. Jayaprakash, M. Kumar, A.C. Pendleton, A. Ganee, A. Fernandez-Sesma, T.M. Moran, and J.G. Wetmur, "Chromosome-Specific and Noisy IFNB1 Transcription in Individual Virus-Infected Human Primary Dendritic Cells," *Nucleic Acids Research,* vol. 35, no. pp. 5232-5241, 2007.
[43] G. Vitale, P.M. van Koetsveld, W.W. de Herder, K. van der Wansem, J.A. Janssen, A. Colao, G. Lombardi, S.W. Lamberts, and L.J. Hofland, "Effects of Type I Interferons on IGF-Mediated Autocrine/Paracrine Growth of Human Neuroendicrine Tumor Cells," *Am. J. Physiology, Endocrinology, and Metabolism,* vol. 296, no. 3, pp. E559-E566, 2009.
[44] A. Donic, M. Falleur-Fettig, and J.M. Skotheim, "Distinct Interactions Select and Maintain a Specific Cell Fate," *Molecular Cell,* vol. 43, no. 4, pp. 528-539, 2011.
[45] H. Kitano, "Biological Robustness," *Nat'l Rev. Genetics,* vol. 5, no. 11, pp. 826-837, 2004.
[46] S.T. Li, L.Y. Wang, M. Berman, Y.Y. Kong, and M.E. Dorf, "Mapping a Dynamic Innate Immunity Protein Interaction Network Regulating Type I Interferon Production," *Immunity,* vol. 35, pp. 426-440, 2011.
[47] M. Recher and K.S. Lang, "Innate (Over)immunity and Adaptive Autoimmune Disease," *Current Topics in Microbiology and Immunology,* vol. 305, pp. 89-104, 2006.
[48] K. Kawamura, N. Kadowaki, T. Kitawaki, and T. Uchiyama, "Virus-Stimulated Plasmacytoid Dendritic Cells Induce CD4+ Cytotoxic Regulatory T Cells," *Blood,* vol. 107, no. 3, pp. 1031-1038, 2006.

Wei Zhang received the BS degree from the China Three Gorges University in 2008 and the MS degree in computational mathematics from Wuhan University in 2011. He is currently working toward the PhD degree at the School of Mathematics and Statistics, Wuhan University, China. His research interests include complex networks, computational intelligence, and system biology.

Xiufen Zou received the BS and MS degrees in computational mathematics and the PhD degree in computer science from Wuhan University, China, in 1986, 1991, and 2003, respectively. She is currently a full professor at the School of Mathematics and Statistics, Wuhan University. Her current research interests include computational intelligence and its applications in complex biological systems. She has published more than 40 academic papers in the aforementioned areas. She was a recipient of the First-Class Prize of the Natural Science Award of Hubei Province, China, in 2005 for her paper "Parallel Evolutionary Optimization and Modeling Algorithms" and the Third-Class Prize of the Science and Technology Progress Award of the National Educational Ministry of China in 1998 for her paper "Parallel Computational Model and Algorithms for Complex System."